AMERICAN SOCIETY FOR MICROBIOLOGY | Molecular and Cellular Biology®

RESEARCH ARTICLE

Multiplication of Ribosomal P-Stalk Proteins Contributes to the Fidelity of Translation

Leszek Wawiórka,[a] Eliza Molestak,[a] Monika Szajwaj,[a] Barbara Michalec-Wawiórka,[a] Mateusz Mołoń,[b] Lidia Borkiewicz,[a] Przemysław Grela,[a] Aleksandra Boguszewska,[a] Marek Tchórzewski[a]

Department of Molecular Biology, Maria Curie-Skłodowska University, Lublin, Poland[a]; Department of Biochemistry and Cell Biology, University of Rzeszów, Rzeszów, Poland[b]

ABSTRACT The P-stalk represents a vital element within the ribosomal GTPase-associated center, which represents a landing platform for translational GTPases. The eukaryotic P-stalk exists as a uL10-(P1-P2)$_2$ pentameric complex, which contains five identical C-terminal domains, one within each protein, and the presence of only one such element is sufficient to stimulate factor-dependent GTP hydrolysis *in vitro* and to sustain cell viability. The functional contribution of the P-stalk to the performance of the translational machinery *in vivo*, especially the role of P-protein multiplication, has never been explored. Here, we show that ribosomes depleted of P1/P2 proteins exhibit reduced translation fidelity at elongation and termination steps. The elevated rate of the decoding error is inversely correlated with the number of the P-proteins present on the ribosome. Unexpectedly, the lack of P1/P2 has little effect *in vivo* on the efficiency of other translational GTPase (trGTPase)-dependent steps of protein synthesis, including translocation. We have shown that loss of accuracy of decoding caused by P1/P2 depletion is the major cause of translation slowdown, which in turn affects the metabolic fitness of the yeast cell. We postulate that the multiplication of P-proteins is functionally coupled with the qualitative aspect of ribosome action, i.e., the recoding phenomenon shaping the cellular proteome.

KEYWORDS ribosomal proteins, ribosomal stalk, ribosome

Received 11 February 2017 **Returned for modification** 11 March 2017 **Accepted** 6 June 2017

Accepted manuscript posted online 12 June 2017

Citation Wawiórka L, Molestak E, Szajwaj M, Michalec-Wawiórka B, Mołoń M, Borkiewicz L, Grela P, Boguszewska A, Tchórzewski M. 2017. Multiplication of ribosomal P-stalk proteins contributes to the fidelity of translation. Mol Cell Biol 37:e00060-17. https://doi.org/10.1128/MCB.00060-17.

Copyright © 2017 American Society for Microbiology. All Rights Reserved.

Address correspondence to Leszek Wawiórka, mniak11@hektor.umcs.lublin.pl, or Marek Tchórzewski, maro@hektor.umcs.lublin.pl.

L.W. and E.M. contributed equally to this article.

At the expense of energy from GTP hydrolysis, translational GTPases (trGTPases) confer the unidirectional trajectory for the translational apparatus, providing at the same time unique timing for individual steps (1, 2). The main landing platform for trGTPases is situated on the large ribosomal subunit called the GTPase-associated center (GAC), and it represents a universally conserved ribosomal element where stimulation of trGTPase catalytic activity takes place (3). The GAC consists of two main elements, a conserved fragment of rRNA called the sarcin-ricin loop (SRL) and a ribosomal stalk composed of ribosomal proteins, which form an oligomeric protein complex (4). The protein part of GAC, the ribosome stalk, can be divided into two functionally and evolutionarily distinct parts, the base of the stalk and its lateral elements. The stalk base is composed of conserved ribosomal proteins uL11 (former names L11 and L12 for prokaryotes and eukaryotes, respectively) and uL10 (former names L10 and P0), which anchor the stalk to the rRNA (5, 6). The lateral part of the stalk is built of dimeric complexes P1-P2 in eukaryotes/archaea or (bL12)$_2$ in prokaryotes (4, 7). Despite the lack of amino acid sequence conservation, the lateral stalk fulfils the same functions and has a similar structural architecture across all domains of life (8). P1/P2 and bL12 proteins are built of two domains. The globular N-terminal domain (NTD) is responsible for dimerization, whereas the highly acidic C-terminal domain (CTD) interacts with trGTPases (9, 10). However, the structure of the CTD in eukaryotes/

archaea and that in prokaryotes are different: in bL12, the CTD has a globular fold, whereas in P1/P2, the CTD is unstructured and may adopt a single short α-helical structure upon binding to trGTPase (3, 11–15). The NTD and CTD are connected through a highly flexible hinge region (16, 17). The flexibility of the hinge and the negative charge of the CTD are critical for the ribosome function, because deletion of this region is lethal for bacterial and yeast cells (18, 19). The bL12 stalk in bacteria is composed of several copies of the same protein bL12; the copy number varies from 4 to 8 depending on the organism (20–22). In eukaryotes, the P-stalk is built of different proteins that belong to two separate groups, P1 and P2, associated as two independent P1-P2 heterodimers (23) on the uL10 protein, forming pentamer uL10-$(P1\text{-}P2)_2$ (5, 7). In *Saccharomyces cerevisiae*, the P1 and P2 groups are further subdivided into four P-proteins (P1A, P1B, P2A, and P2B), forming two heterodimers (P1A-P2B and P1B-P2A) (24). They are bound to the highly specific, helical regions of uL10 within a C-terminal polypeptide, called the P-domain (25–27), and form the pentameric organization uL10-(P1A-P2B)(P1B-P2A) (28). It should be pointed out that the presence of the P-domain alone on the eukaryotic uL10 on the ribosome is sufficient to sustain ribosome functioning, even in the complete absence of P1/P2 proteins (19, 29). The uL10 P-domain contains a highly conservative negatively charged C-terminal tail connected with a flexible linker region resembling an oligopeptide found in P1/P2 proteins, which represents the smallest P-stalk element conferring functionality for the eukaryotic ribosome (25, 30, 31).

Being a very dynamic structure (17), the whole ribosomal stalk eludes structural analyses, including crystallography and cryo-electron microscopy (cryoEM) of bacterial and, especially, eukaryotic ribosomal particles. High-resolution structures of bacterial ribosomes trapped in various states have revealed only a few snapshots of the lateral stalk structure (3, 32, 33). Interactions with trGTPases result in the formation of the so-called Arc-like connection (ALC) between the trGTPase G-domain, uL11 N-terminal fragment, and bL12 CTD (34). It has been proposed that the ALC represents the GAC rearrangement and may play an important role for simulation of GTP hydrolysis by trGTPases. The mechanism of GTP hydrolysis is conserved in all domains of life (35, 36), with the SRL being critical for direct activation of the trGTPases (37, 38). However, the cooperativity of the SRL and both the base and lateral stalk elements has been shown to be pivotal in the stimulation of GTP hydrolysis by trGTPases (39, 40). Kinetic studies of the bacterial translation system suggest that the lateral stalk accelerates GTP hydrolysis by EF-Tu and EF-G by more than 3 orders of magnitude (3, 41), with EF-Tu being the fastest trGTPase (42–45). In the case of eukaryotic P1/P2 proteins, *in vitro* analyses of ribosomes depleted of P1/P2 proteins or a C-terminal domain showed that those structural elements play an important role in the stimulation of GTP hydrolysis of both EF-1A and EF-2 factors and support *in vitro* translation (10, 29, 46–48).

Although the role of the stalk proteins in the stimulation of GTP hydrolysis by various trGTPases is well documented *in vitro*, their exact contribution to the performance of the translational machinery, especially the role of multiplication of the stalk proteins, represents a long-standing question. In this study, we have asked the question how the multiplication of P1/P2 proteins affects the performance of the translational machinery *in vivo*. We used a set of yeast mutants with truncated uL10, which are depleted of one P1B-P2A heterodimer or both P1A-P2B and P1B-P2A heterodimers. We show that P1-P2 heterodimers are dispensable for translation processivity, but the lack of P1/P2 proteins changes the metabolic profile of yeast cells by altering the decoding error frequency. Thus, the multiple P1/P2 proteins are associated with translation accuracy rather than with the speed of translation, and we are providing the first experimental evidence of the physiological relevance of multiplication of P1/P2 proteins.

RESULTS

Phenotypic characterization of cells expressing truncated uL10 protein. The role of P1/P2 proteins is not restricted to the interplay with trGTPases, but they are also

indispensable for proper folding and stable structure acquisition of uL10, which alone is prone to misfolding (49). To avoid the negative effect of uL10 misfolding, we used yeast strains in which the native copy of the uL10 gene was replaced with its truncated variants lacking the P1-P2 heterodimer binding sites (a schematic representation of the native and mutant stalk architectures is shown in Fig. 1A). The analyzed strains contain four (wild type [wt]), two (mutant strain uL10$_{\Delta h2}$), or none (uL10$_{\Delta h1h2}$) of the P1-P2 proteins within the stalk complex. Both mutant strains were viable; however, the uL10$_{\Delta h1h2}$ cells exhibited a slow-growth phenotype (Fig. 1B, leftmost panel). The average doubling time was significantly increased from 95 min for the wild type and uL10$_{\Delta h2}$ strains to 115 min for the mutant uL10$_{\Delta h1h2}$ cells (Fig. 1C). Interestingly, the analyses of the cell cycle progression of logarithmically growing cells revealed perturbations in the yeast strain lacking all P1/P2 proteins on ribosomes. The cell cycle progression in the wild-type yeast cells shows a bimodal distribution reflecting haploid (1N) and diploid (2N) yeast cells, which correspond to the G_1 and G_2/M phases of the cell cycle, respectively. The clearly visible shoulder between the two peaks represents cells in the S phase (Fig. 1D). Quantification of the cell cycle progression statistics indicates that the lack of P1/P2 proteins causes cell cycle arrest or prolongation of the G_1 phase, which is presumably responsible for the observed growth rate reduction. The distribution of the yeast uL10$_{\Delta h2}$ cells between the 1N and 2N peaks represents an intermediate state between the wild type and the uL10$_{\Delta h1h2}$ mutant. The exponentially growing cells of both mutants exhibit a cellular morphology similar to that of the wild type, but the average size of the uL10$_{\Delta h1h2}$ cells was decreased (data not shown). This phenotype resembles the so-called petite phenotype, characteristic for yeast mutant strains with mitochondrial malfunctions leading to respiration defects. Surprisingly, the uL10$_{\Delta h1h2}$ cells were unable to utilize nonfermentable carbon sources, such as ethanol and glycerol (Fig. 1B, two panels on the right). The uL10$_{\Delta h2}$ strain was undistinguishable from the wild-type strain.

Functional characterization of translational machinery deprived of P1-P2 heterodimers. The observation that both uL10$_{\Delta h1h2}$ and uL10$_{\Delta h2}$ strains are viable implies that the uL10 protein mutants are properly assembled on the ribosome. We verified this by detecting truncated uL10 proteins on the ribosomes using specific anti-uL10 antibodies. Quantification of Western blot results using antibodies against uL23 as a control revealed that the ribosomes from the mutant strains contained the same amount of uL10 as the wild-type ribosomes (see Fig. S1 in the supplemental material). As expected, truncation of uL10 changed the architecture of the P-stalk. For the uL10$_{\Delta h2}$ protein variant, P1A and P2B proteins were detected, while uL10$_{\Delta h1h2}$ was devoid of all P1/P2 proteins on the ribosomal particles. This showed that only a specific fraction of P1/P2 proteins (P1A-P2B) was able to bind to uL10$_{\Delta h2}$, whereas their binding to uL10$_{\Delta h1h2}$ was completely abolished, as previously reported (25). Interestingly, no enrichment of P1/P2 proteins with either uL10$_{h2}$ or uL10$_{\Delta h1h2}$ cells was observed within the postribosomal fraction (data not shown), which indicates that the excess of P1/P2 that cannot associate with ribosomes is not accumulated in the cytoplasm. Although the importance of the stalk for translation *in vitro* has been well documented for both prokaryotic and eukaryotic ribosomes, the role of the P-stalk elements for cell fitness *in vivo* has not been studied. First it was checked how the mutations affect translational fitness. We measured the kinetics of [^{35}S]methionine incorporation into newly synthesized polypeptides. The translation was much slower (2-fold) in the uL10$_{\Delta h1h2}$ strain than in the wild-type control cells (Fig. 2A); while the impairment in the uL10$_{\Delta h2}$ cells was much less severe (Fig. 2A), the translational fitness of the uL10$_{\Delta h2}$ and uL10$_{\Delta h1h2}$ strains decreased to up to 85% and 55% of that of the wild type, respectively (Fig. 2A, inset). Next, we analyzed polysome profiles as a very sensitive tool to detect various defects of translation. Surprisingly, the polysome profiles of the mutant and wild-type cells were almost indistinguishable (Fig. 2B to D). The 40S-to-60S ratios, which reflect the balance between ribosomal subunit production, were 0.87 $\pm$ 0.11 for the uL10$_{\Delta h1h2}$ strain, 0.78 $\pm$ 0.11 for the uL10$_{\Delta h2}$ strain, and 0.69 $\pm$ 0.13 for the wild type. The other parameter calculated from the polysome profile, i.e., the so-called polysome-to-

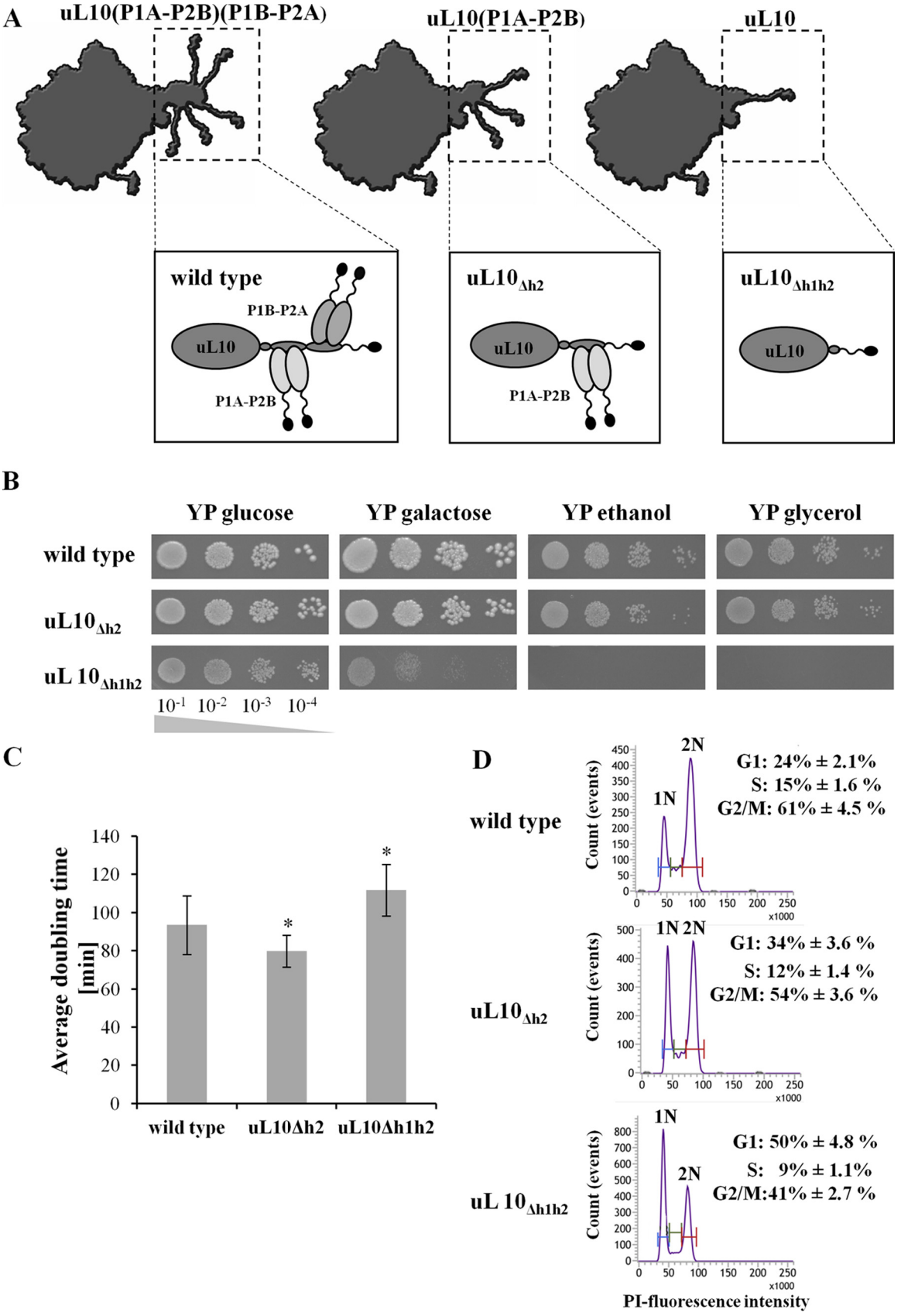

FIG 1 Phenotype analysis of the mutant yeast strains. (A) Schematic representation of the genetically engineered 60S ribosomal subunits with an altered stalk structure: wild type, 60S ribosomal subunit with the intact yeast stalk uL10(P1A-P2B)(P1B-P2A); $uL10_{\Delta h2}$ and $uL10_{\Delta h1h2}$

(Continued on next page)

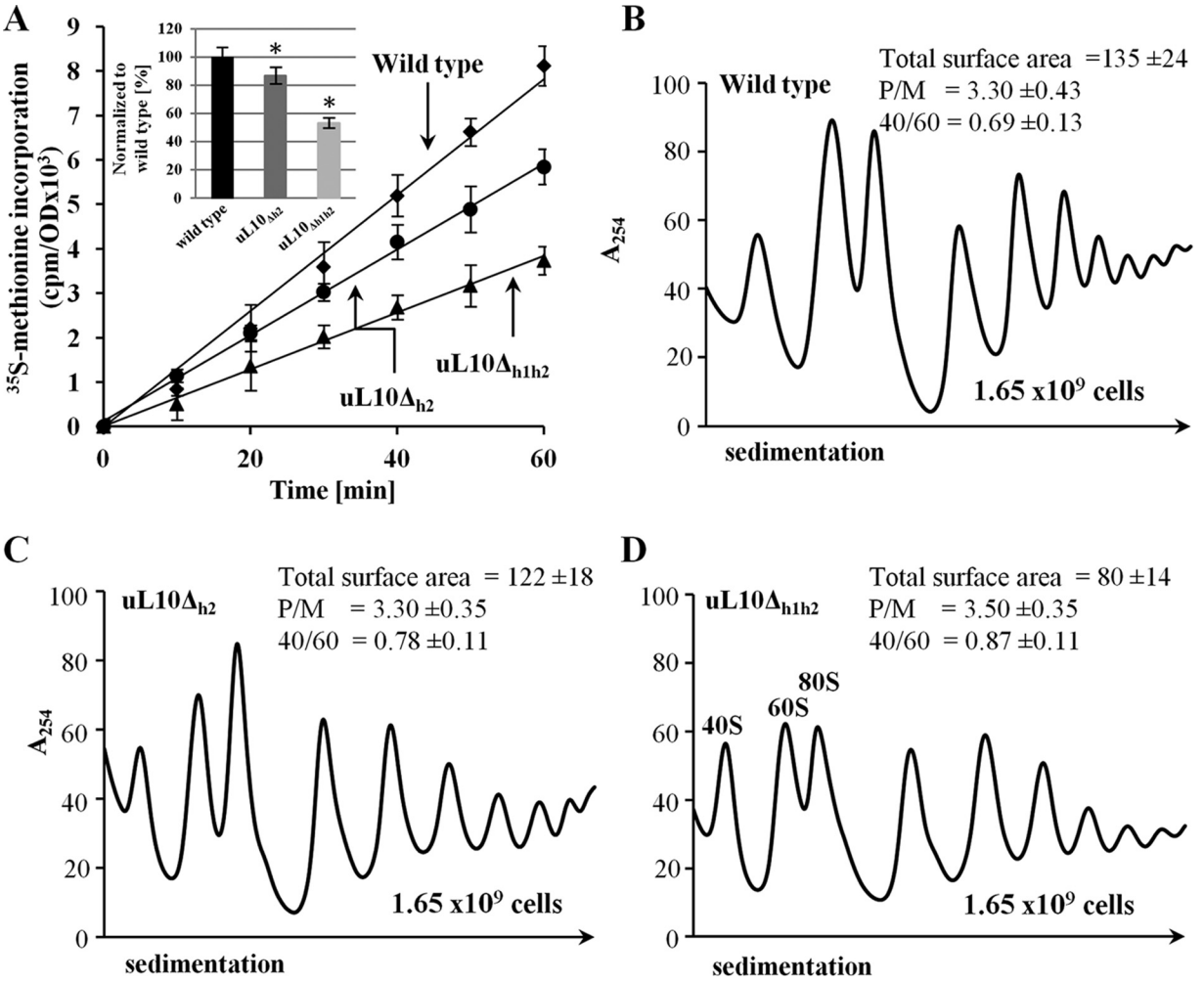

FIG 2 Determination of translational fitness and polysome profile analysis. (A) Measured kinetics of [^{35}S]methionine incorporation into newly synthesized polypeptides, as indicated with arrows. Error bars represent standard deviations obtained from three independent experiments. Inset, translational impairment with respect to the control wild-type cells expressed as 100%, determined based on the slope value for individual graphs. Error bars, standard errors of the mean (SEM) ($n = 3$); *, $P < 0.05$ by Student's t test. (B to D) Polysome profile analyses using equal numbers of cells. Each inset shows the following: the total surface area that was calculated for all 40S, 60S, and 80S peaks and four polysomal peaks, the polysome-to-monosome (P/M) ratio that was calculated for each profile by dividing the area of the first four polysomal peaks by the area of the peak for the 80S monosome, and the 40S/60S ratio. All values, i.e., total surface area, P/M ratio, and ratio of individual 40/60 subunits are shown in each panel as means ± SD ($n = 3$). The sedimentation vector of the ribosomal fractions is indicated by a horizontal arrow, and the optical density value at 254 nm is shown on the y axis; the positions of individual ribosomal subunits are indicated in panel D.

monosome (P/M) ratio, was also not altered considerably in any strains tested (Fig. 2B, C, and D). Additionally, no half-mer fractions, which are a hallmark for defects in 60S biogenesis and/or translation initiation, were detected. Altogether, we observed no signs of significant perturbations in ribosome biogenesis and translation initiation using the polysome profile approach in the mutant cells. It should be pointed out that the polysome profile was determined using equal numbers of cells to compare the amounts of the ribosomal fraction in the mutant strains. The calculated total surface area of the profile showed that the uL10$_{\Delta h1h2}$ strain, having 80 ± 14, has 40% less

FIG 1 Legend (Continued)
mutant strains, 60S with a stalk lacking marginal P1B-P2A or all P1/P2 proteins, respectively; the black blobs represents conserved C-terminal oligopeptides. (B) Growth of mutant yeast strains on various carbon sources. Yeast cells were spotted onto agar plates with YP medium supplemented with various carbon sources as indicated; growth was continued for 3 days. (C) Doubling time determination. The results are presented as the mean ± standard deviation; asterisks indicate statistically significant differences at a P of <0.001 determined using Student's t test. (D) Flow cytometry PI fluorescence intensity histograms of the yeast cell cycle; 1N and 2N represent haploid and diploid cell populations, respectively. The inset shows signal distribution between G_1, S, and G_2/M phases expressed in percentages; the values are means ± SD ($n = 3$).

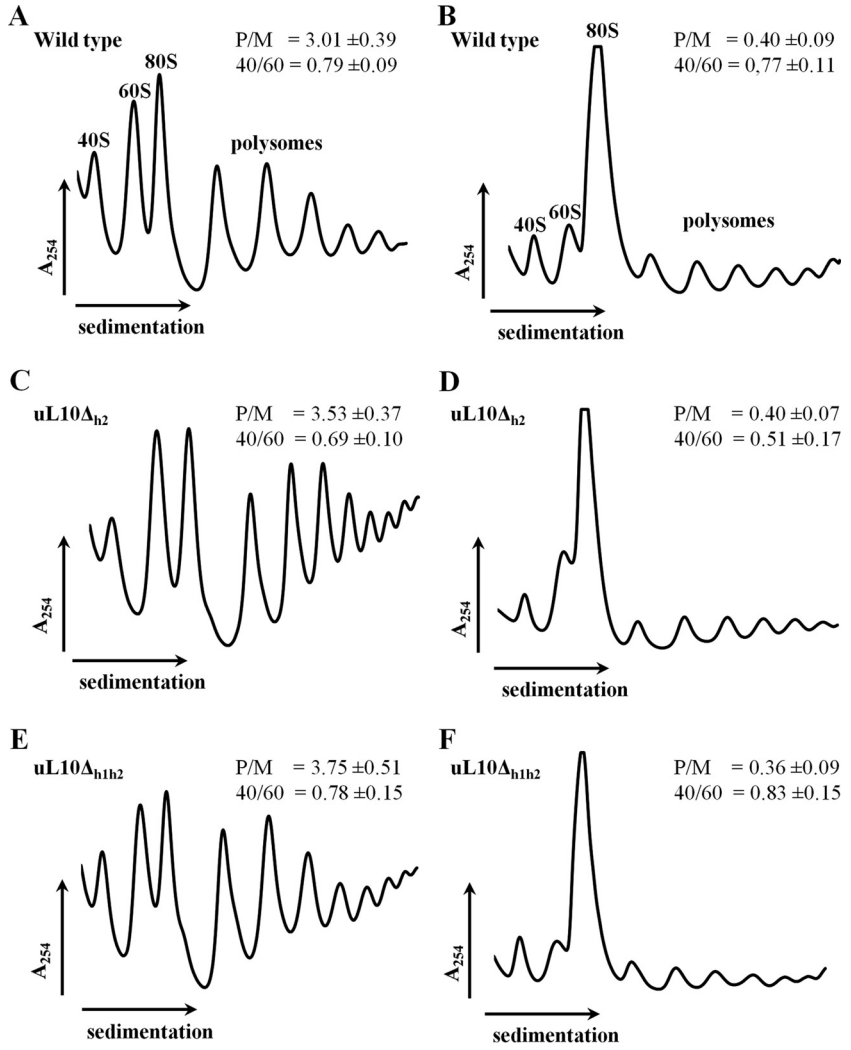

FIG 3 Polysome profile analysis under runoff conditions. (A, C, and E) Control polysome profiles from the wild-type and $uL10_{\Delta h2}$ and $uL10_{\Delta h1h2}$ strains in the presence of CHX. (B, D, and F) Runoff experiments in the absence of CHX. The insets show the polysome-to-monosome (P/M) ratio calculated for each profile by dividing the area of the first three polysomal peaks by the area of the peak for the 80S monosome. The P/M ratio and 40S/60S ratio are shown in each panel as means ± SD (n = 3). The sedimentation vector of the ribosomal fractions is indicated by a horizontal arrow, and the optical density at 254 nm is indicated by a vertical arrow. The positions of individual ribosomal subunits are indicated in panel A.

polysomal fraction than the wild type, with 135 ± 24, and the $uL10_{h2}$ strain, with 122 ± 18 (Fig. 2B to D). This observation is in line with the translational fitness analysis, which showed a significant reduction in the overall kinetics of translation.

To get further insight into postinitiation events during the translation process, we analyzed the polysome profiles under the so-called runoff conditions, when the polysomes are not stalled on mRNA by cycloheximide (CHX). Under such conditions, defects in elongation or termination can be detected. Thus, the cycloheximide was omitted, and the cell extracts were incubated for 20 min at 30°C; under such conditions, wild-type ribosomes are able to complete translation, which is seen as a decrease in the P/M ratio (Fig. 3B, D, and F). If the elongation and/or termination phases are slowed down, ribosomes require more time to complete translation, which should be observed as residual polysome stalling and is reflected in a higher P/M ratio. Surprisingly, the efficiencies of the polysome runoff for the wild-type and P1/P2-depleted ribosomes were similar, which indicates that there is no impairment in the postinitiation steps of translation in the tested strains (Fig. 3B, D, and F). As a positive control, we used the

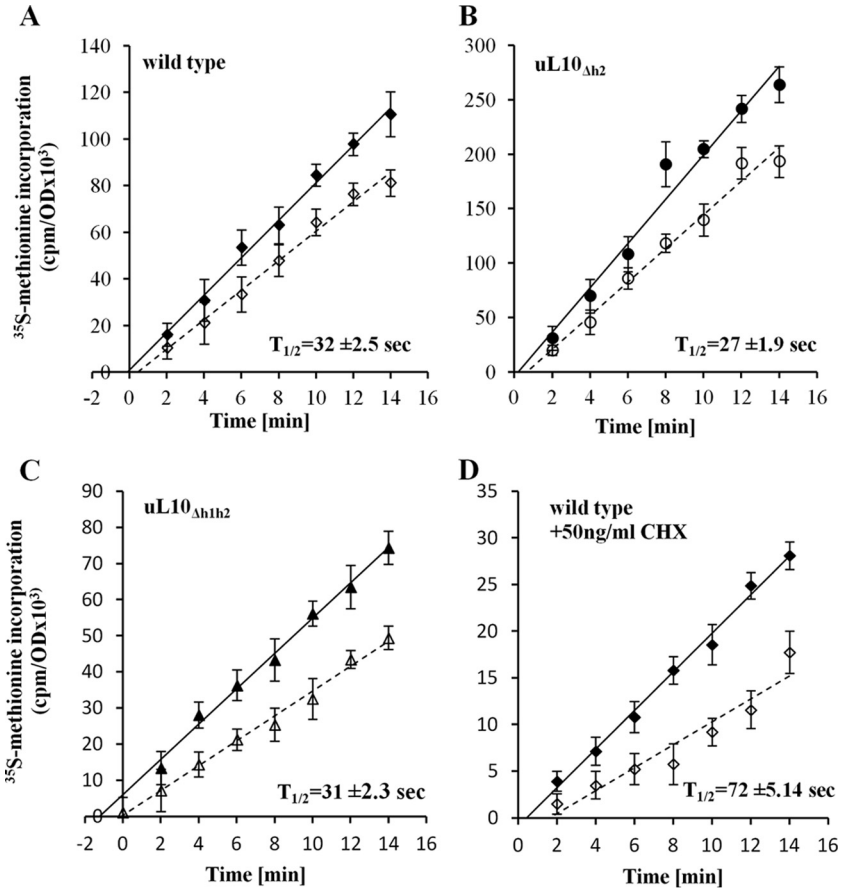

FIG 4 Ribosomal half-transit time. The incorporation of [^{35}S]methionine into total proteins (nascent and completed) (filled symbols) and completed proteins (open symbols) is shown for each strain. The half-transit time was measured as the displacement between two lines by linear regression analysis and is shown in each panel as an inset. $t_{1/2}$ values are means ± SD (n = 3). (A to C) Half-transit times determined for the wild-type (A), uL10$_{\Delta h2}$ (B), and uL10$_{\Delta h1h2}$ (C) strains. (D) Measured half-transit time for the wild-type strain in the presence of a low dose of 50 ng/ml CHX. Error bars represent standard deviations obtained from three independent experiments.

wild-type cells grown at a sublethal cycloheximide concentration, which specifically blocks the elongation of the translation process. We used a concentration of cycloheximide (50 ng/ml) that reduces the translational fitness measured as the [^{35}S]methionine incorporation rate in wild-type cells to the level observed in nontreated uL10$_{\Delta h1h2}$ cells (35% of impairment) (Fig. S2). The polysome profile after the low-dose cycloheximide treatment represented an intermediate state between runoff and classic stalled polysomes, with the P/M ratio calculated as 0.67 ± 0.11 (Fig. S2). This indicates that the reduced number or absence of P1-P2 heterodimers on the ribosomes does not affect the efficiency of either translation elongation or termination. Thus, the translation impairment observed for the uL10$_{\Delta h1h2}$ cells cannot be attributed to the elongation efficiency defect. To validate these unexpected results, the ribosome half-transit time ($t_{1/2}$) was determined for the wild-type and mutant strains. The analysis is based on a comparison of time courses of incorporation of radiolabeled amino acid residues into total (nascent and released) polypeptides and those released from the ribosome. The half-transit time is calculated from the time delay between two lines. This parameter describes the average processivity of the ribosome. The $t_{1/2}$ values for the wild-type and mutant ribosomes were similar (Fig. 4). As a control, we used once again the wild-type cells treated with 50 ng/ml of cycloheximide, a low dose, causing overall translation inhibition similar to the uL10$_{\Delta h1h2}$ level, and the analysis showed that in the case of cells treated with CHX, the $t_{1/2}$ was doubled (Fig. 4D). As no analogous alterations were

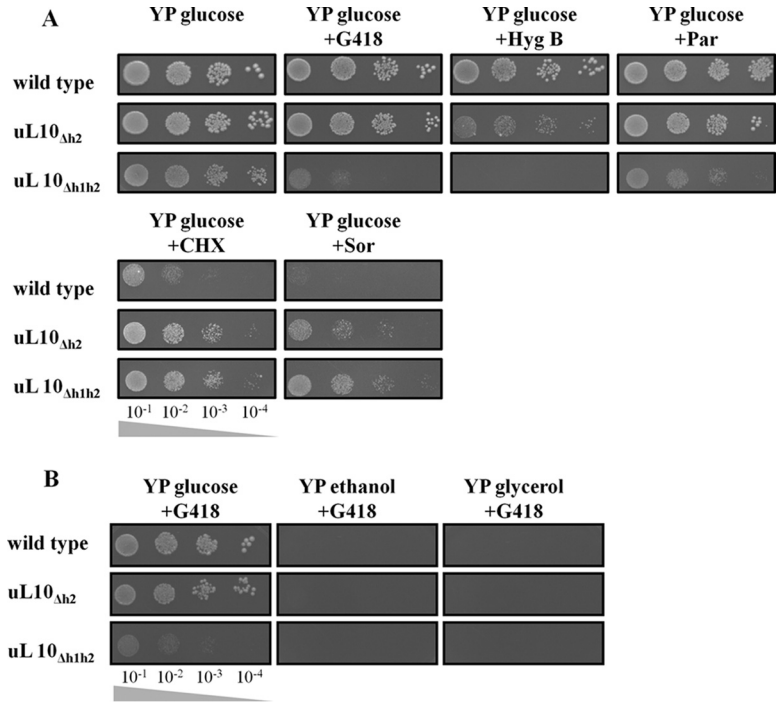

FIG 5 Antibiotic sensitivity test with inhibitors acting on the elongation cycle of protein synthesis. (A) The wild-type and mutant strains were spotted onto YPD agar plates as a serial 10-fold dilution of the original cell culture with an OD_{600} of 0.1 and grown for 3 days. The medium was supplemented with 100 μg/ml G418, 100 μg/ml HygB, 250 μg/ml Par, 0.1 μg/ml CHX, and 2 μg/ml Sor. (B) Growth of wild-type and mutant yeast strains on glucose, ethanol, or glycerol as the only carbon source; the growth medium was supplemented with 100 μg/ml G418. Yeast cells were cultivated as described for panel A.

seen for either the $uL10_{\Delta h2}$ or $uL10_{\Delta h1h2}$ yeast strain, it can be concluded that ribosomes depleted of P1/P2 proteins drive the translation elongation process *in vivo* to the same extent as the wild type.

P1-P2 heterodimer deficiency alters the antibiotic sensitivity of the mutant yeast strains. Next, we checked the response of the yeast strains with ribosomes lacking P1/P2 proteins to specific translation inhibitors. We have screened the sensitivity of the strains to numerous antibiotics acting on initiation and elongation, and we found that aminoglycoside antibiotics, able to interfere with the first step of the elongation cycle, i.e., mRNA decoding (paromomycin [Par], hygromycin B [HygB], and Geneticin G418), exerted the strongest negative effect on mutant growth. Additionally, we have also found an effect of cycloheximide and sordarin (Sor), which act on the subsequent step of elongation, namely, the tRNA-mRNA translocation. The $uL10_{\Delta h1h2}$ (but not wild-type or $uL10_{\Delta h2}$) cells were hypersensitive to the decoding inhibitors, with the strongest effect shown for the eukaryote-specific G418 and hygromycin B (Fig. 5A, upper panel). The hypersensitivity of the analyzed strains to aminoglycosides might suggest an additive effect of decoding perturbations and P1/P2 deficiency. This, in turn, implies that P-proteins might be involved in the maintenance of translational accuracy. Interestingly, the lack of P1/P2 proteins decreases the sensitivity to sordarin, an inhibitor of EF-2-dependent translocation. The $uL10_{\Delta h1h2}$ strain is resistant to a concentration of sordarin that is lethal to wild-type cells (Fig. 5A, lower panel). Furthermore, the $uL10_{\Delta h1h2}$ and $uL10_{\Delta h2}$ mutant strains showed elevated resistance to cycloheximide. Striking data were obtained using a nonfermentable carbon source, i.e., ethanol or glycerol, in the presence of G418. As shown above, the $uL10_{\Delta h1h2}$ mutant strain is not able to utilize ethanol or glycerol and the growth of the strain is blocked. In the presence of G418, the wild-type strain loses its ability to utilize ethanol or glycerol, exhibiting/mimicking the $uL10_{\Delta h1h2}$ mutant phenotype grown on ethanol- or glycerol-based medium (Fig. 5B).

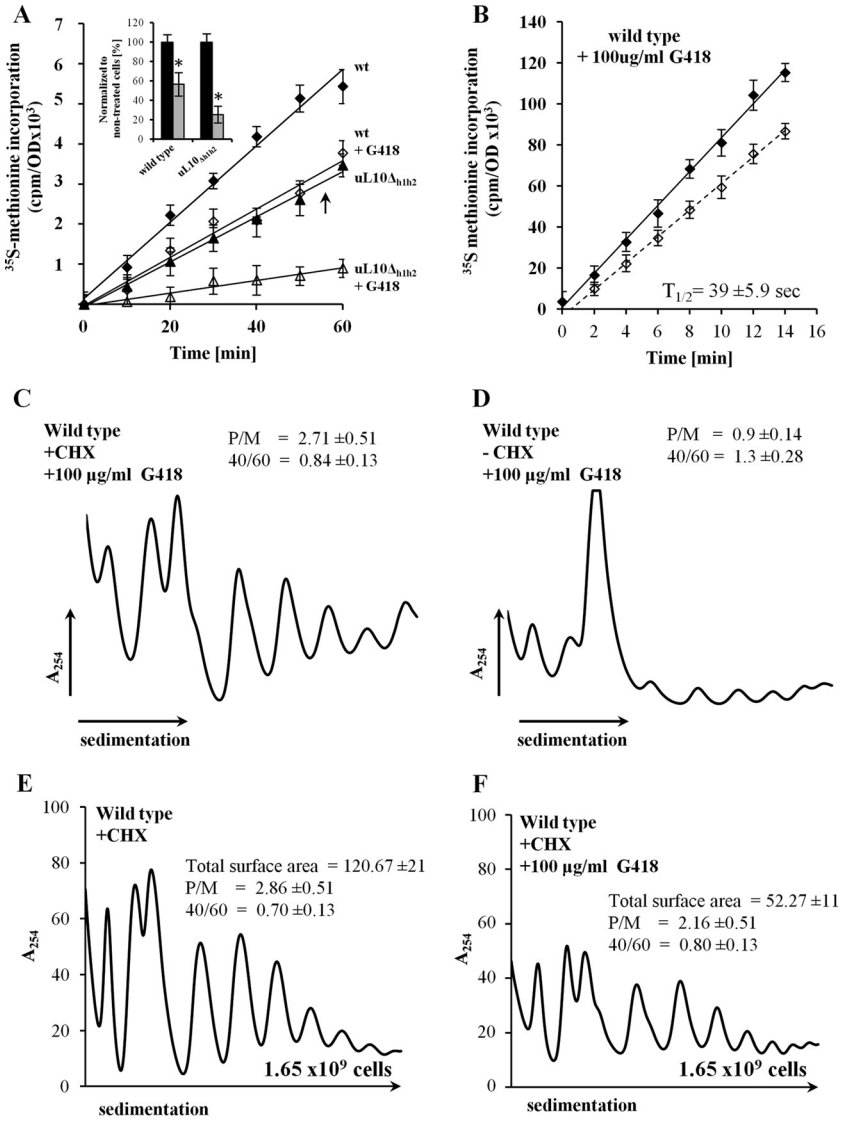

FIG 6 Effect of G418 on the BY4741 wild-type strain. (A) Translational fitness determined as a function of [^{35}S]methionine incorporation in the presence of a sublethal dose of G418 (100 μg/ml). wt, wild-type strain. Error bars represent standard deviations obtained from three independent experiments. Inset, translational efficiency normalized to nontreated cells; error bars, SEM ($n = 3$); *, $P < 0.01$, Student's *t* test. (B) Half-transit time determined for the wild-type strain in the presence of 100 μg/ml G418. (C) Polysome profile from wild-type cells grown in the presence of 100 μg/ml G418 and stalled with CHX. (D) Polysome profile analysis under runoff conditions. (E and F) Polysome profile analyses using equal numbers of cells. The analysis was done as described in the legend to Fig. 2.

To show the exact effect of G418, a sublethal concentration (100 μg/ml) was used to quantify the effect on translational efficiency as a function of [^{35}S]methionine incorporation. G418 reduced the [^{35}S]methionine incorporation by 40% in the wild type and by 80% in the uL10$_{\Delta h1h2}$ mutant (Fig. 6A, inset). To functionally link the aforementioned phenomena with translationally active ribosomes, the ribosome half-transit time was determined for the wild-type strain exposed to G418. The $t_{1/2}$ was modestly increased, to 39 $\pm$ 5.9 s (Fig. 6B), indicating that G418 does not significantly affect elongating ribosomes. Furthermore, in the presence of G418, the polysome profiles showed that this antibiotic did not significantly alter the overall profiles (Fig. 6C). Also, analysis under runoff conditions showed the disappearance of the polysomal fraction (Fig. 6D), indicating that G418-induced misincorporation resembles the translational apparatus behavior found in the uL10$_{\Delta h1h2}$ cells. Additionally, the polysome profile was

determined using equal numbers of cells to compare the amounts of the ribosomal fraction between the nontreated and G418-treated cells. The calculated total surface area of the polysomes showed that the wild-type strain grown in the presence of G418 has 60% less ribosomal fraction than the untreated strain (Fig. 6E and F), once again underscoring the similarities between the G418-treated wild-type cells and the $uL10_{\Delta h1h2}$ mutant strain.

P1/P2 proteins affect translational accuracy. The hypersensitivity of the $uL10_{\Delta h1h2}$ strain to aminoglycoside antibiotics that induce translational errors suggests a potential defect in the maintenance of translational accuracy. In order to test this idea, we used a dual-luciferase reporter assay. We measured the activities of two different luciferase reporter enzymes (*Renilla* and firefly), which are expressed as a single hybrid protein harboring full enzymatic activity of both enzymes. The specific modifications within the downstream luciferase (firefly) gene make its activity dependent on the occurrence of a specific type of translation errors. The incorporation of a near-cognate amino acid instead of a cognate one is quantified in a misincorporation assay and is a gauge of decoding errors during elongation. The readthrough assay quantifies stop codon suppression, which reflects the frequency of ribosome errors during termination. To quantify the defects in reading frame maintenance, the frequency of -1 and $+1$ programmed ribosomal frameshifting (PRF) was determined using an analogous system, in which a specific -1 PRF signal derived from yeast L-A virus or a $+1$ PRF signal derived from a Ty1 retrotransposon was introduced between the two luciferase genes (50). Using the dual-luciferase reporter assays, we found a significant increase in the frequency of misincorporation and readthrough events. Especially, we focused on misreading, because the $uL10_{\Delta h1h2}$ strain is hypersensitive to aminoglycoside antibiotics, indicating an additive effect. We used the dual-luciferase-based experimental approach to test the misincorporation frequency in mutant cells. As the misreading of some near-cognate codons may vary by an order of magnitude and some mutations are not fully deleterious to the luciferase enzyme (51), we applied several well-developed experimental systems. The first system utilizes the mutations in position 245 of the firefly reporter, using two near-cognate codons, CGC and CAG (52). We also used an additional mutation within the firefly gene, namely, the near-cognate codon AGC encoding amino acids at position 218 of firefly protein (53). Using the two systems, we determined that the frequency of misreading errors increased up to 2-fold for the $uL10_{\Delta h2}$ strain and more than 3-fold for the $uL10_{\Delta h1h2}$ strain, depending on the system used (Fig. 7). We also used the noncognate codons (CGA_{245} and TCT_{218}) as negative controls, where the measurement showed that the mutant strains had no unspecific defects at the initial selection step of decoding (Fig. 7). The obtained data once again underscore the fact that the mutant strain lacking all P1/P2 proteins has a high propensity to misincorporate the near-cognate codon and indicate that the accuracy of the decoding step is compromised by a reduction in the copy number of P1-P2 heterodimers. As a key reference, we used wild-type cells treated with the antibiotic G418, which specifically affects ribosomal decoding and stimulates misreading (53, 54). Additionally, our phenotypic/biochemical analyses showed that the treatment of the wild-type cells with 100 μg/ml of G418 mimicked the behavior of the $uL10_{\Delta h1h2}$ mutant (Fig. 5 and 6). Thus, the wild-type cells were treated with G418 (at concentrations of 100 and 200 μg/ml). A significant increase in the ribosome error frequency at the near-cognate codons was observed (Fig. S3); the analyses performed using noncognate codons showed no changes in error frequency (Fig. S3). Thus, the combination of P1/P2 deprivation with chemical reduction of ribosomal accuracy might elevate the translation error rate over the lethal level, which explains the hypersensitivity of the $uL10_{\Delta h1h2}$ (but not $uL10_{\Delta h2}$) strain to aminoglycosides. The frequency of $+1$ PRF was also affected by the lack of the P1/P2 proteins (1.5-fold increase), whereas a frequency of -1 PRF was not affected by the mutation (Fig. 8). These results indicate that the multiplication of P1/P2 proteins has an unexpected, never-ascribed role in maintaining fidelity rather than conferring the speed of translation.

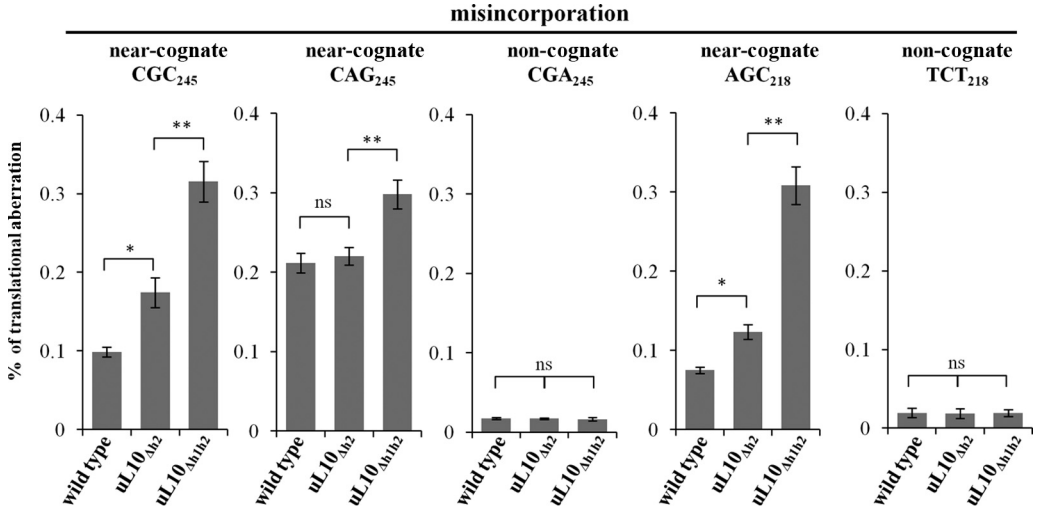

FIG 7 Misincorporation analysis using a dual-luciferase reporter assay. CGC_{245}, CAG_{245}, and AGC_{218} describe near-cognate codons at positions 245 and 218 of the firefly reporter enzyme; CGA_{245} and TCT_{218} represent the noncognate codons used at the respective positions within the firefly reporter enzyme. All data are presented as the percentage of translational aberration; error bars represent standard deviations. Statistical significance of differences assessed using the one-way analysis of variance (ANOVA) method, followed by the *post hoc* Tukey honest significant difference (HSD) test, is indicated by asterisks: *, $P < 0.01$; **, $P < 0.001$; ns, not significant.

Effect on cell metabolism. In functional studies, the defective phenotype caused by gene mutation/deletion is usually restored by the ectopic expression of the wild-type copy of the mutated gene. Accordingly, we tested whether the defects caused by the uL10 mutations can be restored by the plasmid-borne expression of the full-length uL10 gene in the genetic background of the $uL10_{\Delta h1h2}$ strain. Unexpectedly, the presence of the native copy of the uL10 protein only modestly restored the slow-growth phenotype of the $uL10_{\Delta h1h2}$ strain (Fig. 9A, upper panel). To rule out the possibility that this was caused by the very low expression of uL10, the abundance of uL10 was quantified by Western blotting. Both full-length and truncated uL10 variants were detected in the ribosome fractions and free in cytoplasmic fractions (Fig. 9B). This suggests that there were no differences in the expression levels of the wild-type and mutated uL10 proteins or in their affinity for ribosomes. Thus, it is likely that the presence of ribosomes depleted of P1/P2 proteins, rather than their deficiency itself, exerts a detrimental effect on overall cell metabolism. To verify this hypothesis, an inverse approach was applied. The gene for the truncated $uL10_{\Delta h1h2}$ protein was

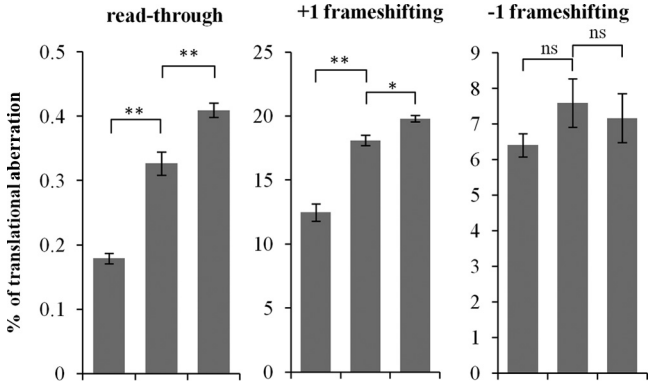

FIG 8 Read-through and −1/+1 programmed frameshifting (PRF) analysis using a dual-luciferase reporter assay. All data are presented as the percentage of translational aberration. Error bars represent standard deviations. Statistical significance of differences assessed using one-way ANOVA method, followed by the *post hoc* Tukey HSD test, is indicated by asterisks: *, $P < 0.01$; **, $P < 0.001$; ns, not significant.

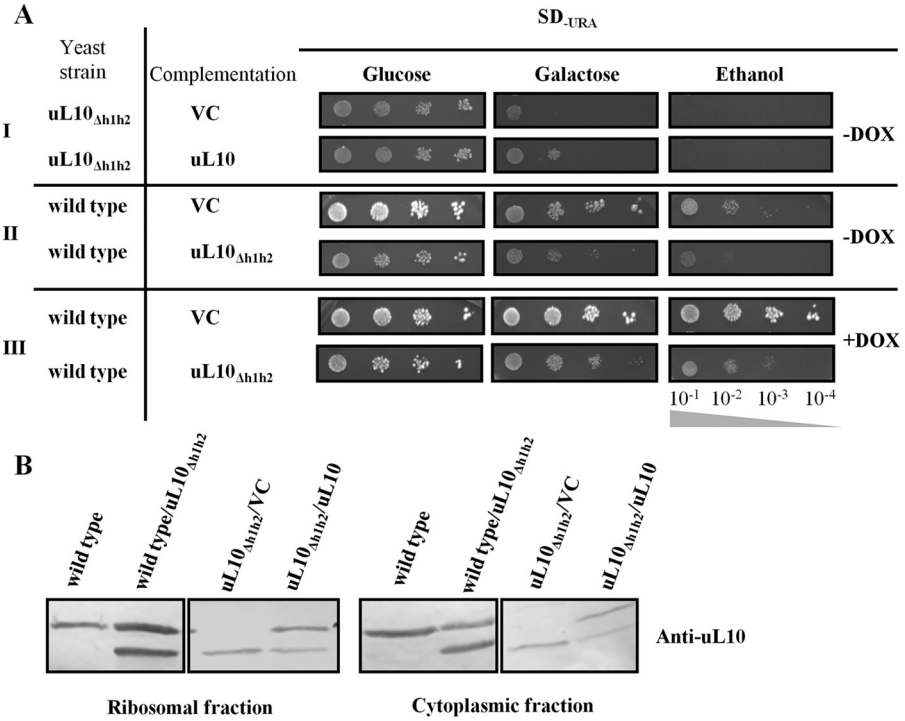

FIG 9 Complementation experiment of the $uL10_{\Delta h1h2}$ mutant strain and wild-type cells. (A) Growth of $uL10_{\Delta h1h2}$ yeast mutant and wild-type strains on SD_{-Ura} medium supplemented with various carbon sources; the cells were transformed with an empty vector (vector control [VC]) or with a vector bearing genes for full-length uL10 or truncated $uL10_{\Delta h1h2}$; yeast cells were spotted onto agar plates and cultivated for 3 days in the absence or presence of doxycycline (DOX) in order to induce or suppress expression of the uL10 or $uL10_{\Delta h1h2}$ genes. (B) Western blotting of the full-length and truncated uL10 protein using specific polyclonal anti-uL10 antibodies; two fractions were analyzed, the total ribosomal fraction and the cytoplasmic fraction deprived of ribosomes.

ectopically expressed in the wild-type strain, using the pCM190 vector. In such cells, the truncated protein effectively competed with the native uL10 and was found in the ribosomal and cytoplasmic fractions, as shown by Western blots (Fig. 9B). The wild-type cells with plasmid-borne expression of $uL10_{\Delta h1h2}$ (induced by the absence of doxycycline [DOX]) displayed a reduced growth rate in both glucose- and galactose-based media (Fig. 9A, middle panel). Moreover, such cells were unable to utilize ethanol as the only carbon source, as was the case in the $uL10_{\Delta h1h2}$ yeast mutant. Since the gene for the $uL10_{\Delta h1h2}$ variant is under the control of the tetO/tTA regulatory system, it is possible to regulate its expression (−DOX, stimulate expression; +DOX, repress expression). Both the growth rate and the ability to utilize alternative and nonfermentable carbon sources were restored by the $uL10_{\Delta h1h2}$ repression, which indicates that the expression of $uL10_{\Delta h1h2}$ exerts a dominant negative effect on yeast cells (Fig. 9A, lower panel, +DOX).

DISCUSSION

The ribosome stalk, being an integral part of the GAC, constitutes an interacting platform with trGTPases, which might be considered a molecular propeller driving the process of translation (1, 4, 6, 7). A unique feature of the ribosomal stalk is the multiplication of all stalk proteins that share the same negatively charged, highly conserved C-terminal domain, regarded as the main interface interacting with trGTPases (8, 9, 55). In eukaryotes, pentameric architecture is favored, and thus five such oligopeptides are present, one from each of the P1, P2, and uL10 proteins. Although all five C termini facilitate the full translational activity of ribosomes *in vitro*, the presence of only one is sufficient to sustain cell viability (19, 46), thus raising the question about the role of multiple stalk proteins and the contribution of these individual C-terminal protein elements to the ribosomal action.

P1/P2 proteins are dispensable for the translational speed *in vivo*. The kinetic experiments with bacterial ribosomes unequivocally revealed that the binding of trGTPases, the rate of GTP hydrolysis, and subsequent inorganic P_i release are slowed down upon depletion of the lateral bL12 stalk elements (3, 41, 45, 56). These results were supported by the structural analyses, which showed specific interactions between the stalk and trGTPases (32–34, 39, 40, 57–59). Thus, in bacteria, the CTD of the bL12 stalk protein recruits trGTPases and takes part in stimulation of GTP hydrolysis; however, its direct molecular contribution remains elusive (60). Analogous experiments using a eukaryotic/archaeal system confirmed that P1/P2 proteins are involved in binding and stimulation of trGTPases, underlining the common evolutionary role of the ribosomal stalk, despite structural differences (10, 46, 47). Accordingly, our initial analyses showed that the overall translation efficiency measured *in vivo* was reduced upon deprivation of ribosomal P1/P2 dimers. These quantitative translational perturbations were reflected by the observed slow-growth phenotype, which can be attributed to the lower number of translating ribosomes in the $uL10_{\Delta h1h2}$ mutant strain. However, these quantitative variations do not fully explain the phenotype behavior of the mutant strain. As already noted, the lack of P1/P2 proteins may exert a regulatory effect on yeast cell growth. The quadruple disruptant strain, in which all genes for P1/P2 proteins were deleted, exhibited a slow-growth phenotype, cold sensitivity, and inability to sporulate (30), suggesting that fluctuations within the number of P1/P2 proteins may change the yeast metabolic profile. Our analyses showed that the slow-growth phenotype is mainly related to the cell cycle arrest at the G_1 phase resulting in increased doubling time. This is in agreement with the previous observation showing that changes in the stalk architecture cause fluctuations in the yeast proteome, indicating a regulatory role of P-proteins in the cellular protein profile (30). Interestingly, the analysis of the polysome profiles, including runoff conditions and the ribosome half-transit times, suggests that the efficiency of none of the particular steps of translation (initiation, elongation, or termination) was specifically affected by the P1/P2 depletion. These two seemingly inconsistent lines of evidence do not exclude each other. Even if the GTP hydrolysis and polymerizing activity on ribosomes lacking P1/P2 proteins is slower, as shown *in vitro* (29, 46), the residual activity of ribosomes with the uL10 protein only seems to be sufficient to support the adequate performance of the translational machinery *in vivo* and the yeast cell growth.

P1/P2 proteins increase translational accuracy. The most striking effect of the P1/P2 depletion found in our study is the increase in the misreading frequency, a phenomenon that has never been associated with the P-proteins and stands in opposition to a previous report, which showed that P-proteins are not involved in maintaining the accuracy during translation (30). As we have shown by the dual-luciferase reporter assay, the disturbance in the stalk architecture affects in particular the process of decoding, the qualitative aspect of translation, i.e., missense errors, read-through, and +1 PRF. The discrepancies between our report and the data published previously (30) arise from the different experimental approaches. Remacha et al. used an *in vitro* translation system or an assay based on the single reporter β-galactosidase, both of which are much less sensitive than ours, and they also used a double disruptant strain with trimeric stalk architecture, which, as we have shown, is much less prone to decoding error. Our analyses with the dual reporter system are supported by the observation that the yeast mutant lacking P1/P2 proteins is hypersensitive to several aminoglycoside antibiotics affecting ribosome decoding, exhibiting a synergistic effect between the defect of decoding arising from P-protein deficiency and the aminoglycosides used. Importantly, we have found a positive correlation between the P1/P2 copy number on the ribosome and the effect on the translation accuracy. The depletion of one dimer resulted in a moderate defect, whereas the depletion of two dimers caused a severe increase in the ribosome error rate. These results suggest a role of the multiplication of P1/P2 proteins in translation, as ribosomal elements contribute mainly to translational fidelity. In contrast, the reported effects on

the rate of GTP hydrolysis catalyzed by EF-2, shown in the multiple turnover assay, and on the efficiency of *in vitro* polypeptide synthesis appear not to be physiologically relevant *in vivo* (22, 46, 47), as no defect in the efficiency of elongation was observed *in vivo*. Accordingly, depletion of the P1/P2 proteins on the ribosomal stalk exerts a strong effect on the decoding process at both the elongation and termination levels, which in turn affects translational fitness.

Importantly, treatment of the wild-type cells with the G418 antibiotic exerts a similar effect, where loss of translation accuracy leads to a slowdown of translation efficiency but cannot be seen in other translational assays *in vivo* (polysome profile, runoff, ribosome half-transit time). However, the most striking evidence linking ribosome decoding with regulatory function is the observed phenotype of the yeast mutant, which displayed an inability to grow on nonfermentable carbon sources. The same effect was also recorded for the wild-type cells treated with G418, mimicking the effect observed in the mutant strain. Thus, this implies that changes in the decoding error rate may have an effect on mitochondrial metabolism, hampering aerobic respiration and implicating the ribosomal decoding error rate as a regulatory element. Interestingly, the presence of ribosomes depleted of P1/P2 exerts a dominant negative effect on the wild-type cells, suggesting that a small fraction of altered ribosomes may exert a significant metabolic effect, at the same time showing that perturbations within the stalk (already observed as exchangeability of P-proteins [61]) may contribute to the heterogeneity of the translational machinery and appearance of specialized ribosomes.

Rationale of P1/P2 multiplication. The kinetic experiments showed that the association of trGTPases with ribosomes takes place much more rapidly than that calculated for the random encounter mechanism (62, 63). Thus, it was proposed that the ribosomal stalk might be a key player increasing the trGTPase binding affinity to the ribosome over this diffusion barrier (3, 44). Since the architecture of the GAC, including the stalk, is conserved (but having specificity for prokaryotic and eukaryotic cells), the mechanism of trGTPase recruitment to the ribosome is considered to be universal. Thus, the defect in binding of trGTPases to the ribosome should affect their function in a similar fashion in prokaryotes and eukaryotes. In such a situation, EF-2-catalyzed translocation should be affected to the same extent as decoding, because elongation consumes equal numbers of eEF-2- and eEF-1A-dependent steps. Interestingly, such a situation was indeed described for uL11-depleted yeast cells (64). Since uL11 is present on the ribosome in a single copy, ribosomes lacking this protein were equally defective in all trGTPase dependent steps, including ribosome biogenesis, subunit joining, translation elongation, and termination, and especially affecting central ribosomal activity, the elongation cycle, which was depicted as perturbations in misincorporation, and -1 and $+1$ PRF (64). The situation is more complex in the case of P1/P2 proteins that exist on the ribosome in multiple copies. Recent structures of various trGTPases trapped on bacterial ribosomes revealed that only one CTD (out of four) of analogous bL12 proteins interacts with the G domain of trGTPases (33, 40, 59). Thus, it can be assumed that only one C-terminal region of stalk proteins is indispensable and sufficient for stimulation of each trGTPase. In this work, we have shown that the depletion of all P1/P2 proteins (leaving only one C terminus on the ribosome, situated on the uL10 protein) has no effect on ribosome biogenesis, subunit joining, and translocation *in vivo*. However, the accuracy of decoding, one of the major ribosomal activities, turned out to be strictly dependent on the P1/P2 copy number. Taking into consideration previous data showing that the increase in the P1/P2 copy numbers present on the ribosome facilitates efficient GTP hydrolysis *in vitro*, we can assume that the efficiency of GTP hydrolysis by trGTPases *in vivo* is also dependent on the number of C termini. Accordingly, the reduction in the number of P1/P2 proteins is likely to reduce the rate of GTP hydrolysis *in vivo* for all trGTPases to a similar extent. However, the physiological consequences of an analogous delay in GTP hydrolysis during ribosome biogenesis, subunit joining, or even translocation seem to be indiscernible. Thus, if the biochemical mode of action of P1/P2 is the same for all trGTPases, what makes this physiological difference? The

answer is time. As shown previously in the bacterial system, the rates of GTP hydrolysis differ significantly between the individual trGTPases, ranging from 0.1 s^{-1} for RF3 (65), 36 s^{-1} for IF2 (66), 250 s^{-1} for EF-G (67), and up to >500 s^{-1} for EF-Tu (42). As we did not notice any defect in initiation, termination, or even translocation *in vivo*, it is tempting to speculate that the delay in GTP hydrolysis caused by the reduction in the number of ribosomal stalk C termini does not influence the overall performance of the ribosome during these steps of translation. In contrast, there is a high energetic demand for ribosomal decoding to be very rapid. The GTPase activation brings the ribosome into a state with unequal probabilities for cognate and near-cognate codon incorporation, where the near-cognate dissociation rate is substantially increased in comparison to cognate codon incorporation (42). Thus, the transition from the inactive to active GTPase state is very rapid, underscoring the fact that the ternary complex is adjusted to respond to cognate codon-anticodon duplex interaction immediately after recognition of the duplex by the decoding center. Accordingly, the fast interplay of the stalk and EF-Tu/eEF-1A might be regarded as an additional ribosomal element responsible for correct codon-anticodon sensing and timing of the GTPase activation, providing high precision of initial selection. The kinetic model of decoding assumes that the prolonged persistence (pausing) of the near-cognate ternary complex in the ribosomal A site may lead to misreading, as the probability of GTP hydrolysis increases with the time the ternary complex spends on the ribosome. Therefore, the GTPase activation induced by cognate codon-anticodon pairing within the decoding center needs to be very rapid, and the exceptionally high rate of EF-Tu/eEF-1A can be ensured only by multiple copies of the P-proteins.

Additional evidence supporting our idea is the observed increase in +1 PRF, whereas −1 PRF is unchanged. The proposed model for PRF indicates that +1 PRF takes place when the ribosomal A-site is empty and the P-site is occupied (decoding step), whereas −1 PRF is promoted when the ribosome adopts a "rotated" state with both A- and P-sites occupied (translocation step) (68). Thus, the increase in +1 PRF indicates that the lack of P1/P2 proteins exerts a dominant effect on the posttranslocation state of the ribosome, which is related to ribosome interplay with the GTP–eEF-1A–aatRNA ternary complex. Most likely, the lack of P1/P2 proteins delays the time of this interaction and consequently increases the probability of +1 PRF.

Thus, as we have shown, perturbations within the stalk structure, namely, the reduction of lateral stalk elements, reduce precision of translation. Accordingly, we postulate that the primary molecular function of the multiplication of C termini within the ribosomal stalk involves increasing the interplay efficiency of eEF-1A with the ribosomal GAC, which drives proper cognate versus near-cognate discrimination during the initial selection step of decoding. Thus, the main functional role of the multiple elements of the P-stalk is involvement in control of translational accuracy.

MATERIALS AND METHODS

Genetic manipulations, plasmid construction, and cell growth. The $uL10_{\Delta h2}$ and $uL10_{\Delta h1h2}$ mutant strains were constructed on the basis of BY4741 (*MAT***a** *his3Δ1 leu2Δ0 met15Δ0 ura3Δ0*) (Fig. 1A), as described previously (25). The plasmid used for ectopic expression of the full-length and truncated form of the uL10 protein was constructed based on the pCM190 yeast expression vector. The DNA sequences of uL10 genes were PCR amplified using genomic DNA as a template from the wild-type strain (full-length uL10) and from the $uL10_{\Delta h1h2}$ strain for truncated uL10. The genes were subcloned into a 2μm pCM190 vector using unique BamHI/NotI restriction sites. The expression of the respective genes was driven by a tetO-CYC1 promoter and controlled under a tTA activator. The correctness of all genetic constructs was verified by DNA sequencing.

For spotting experiments, the cells were grown with vigorous shaking to the logarithmic phase of growth (optical density at 600 nm [OD_{600}] = 1 to 2) in yeast extract-peptone-dextrose (YPD) or an appropriate selective medium and then diluted to an OD_{600} of 0.1. The cell suspensions were serially 10-fold diluted and subsequently spotted onto agar plates supplemented with the concentrations of antibiotics shown in the Fig. 5 legend or containing different carbon sources: glucose, 2%; galactose, 2%; ethanol, 2%; or glycerol, 2%. The cells were grown at 30°C for up to 3 days.

Determination of mean doubling time. The mean doubling time was calculated for each analyzed cell as described previously (69). The doubling time was calculated during the determination of the reproductive potential. The times of the first two reproductive cycles were not taken into account (the first and second doubling times are longer than those of older cells). The data

represent the mean values from three independent experiments (with 40 cells used in each experiment) with a mean standard deviation (SD). Statistically significant differences were taken at a P of $\leq$0.001 using the t test.

Polysome profile analysis and immunoblotting. Polysome profiles were obtained by 7-to-47% sucrose gradient centrifugation of the total cell extracts. The cells were grown to an OD_{600} of 0.4 to 0.6 in YPD or an appropriate minimal medium (SD minimal medium) and treated with cycloheximide (CHX) (final concentration, 100 μg/ml) for 20 min to block further protein synthesis. The cells were harvested by centrifugation, resuspended in lysis buffer (10 mM Tris-HCl [pH 7.5], 100 mM NaCl, 30 mM $MgCl_2$, 100 μg/ml CHX, 1 mM phenylmethylsulfonyl fluoride [PMSF], 6 mM β-mercaptoethanol, 1 nM pepstatin A, 10 nM leupeptin, 10 ng/ml aprotinin, 200 ng/ml heparin, and RNase inhibitor [Sigma-Aldrich]), and disrupted by vigorous shaking with glass beads at 4°C. The cell lysate was cleared by centrifugation at 12,000 rpm (rotor 12154-H; Sigma). Fifteen OD_{260} units were loaded on each sucrose gradient, centrifuged for 4.5 h at 26,500 rpm at 4°C in an SW32Ti rotor (Beckman-Coulter), and analyzed using an ISCO Brendel density gradient fractionator. To obtain polysomal fractions from equal numbers of cells, yeast strains were grown as described above, and 1.65×10^9 cells were collected for subsequent polysome preparation, in accordance with the procedure described above and with all standardized steps to ensure the uniform preparation of ribosomal fractions. For the polysome runoff experiment, the polysomes were not preserved by CHX treatment, and accordingly, CHX was omitted from the lysis buffer. The cell extracts were incubated for 20 min at 30°C to complete the elongation round. In order to obtain the polysome profile in the presence of G418, the wild-type cells were grown in YPD supplemented with 100 μg of G418, at an OD_{600} of 0.4 to 0.6, and the polysomes were stalled with 100 μg/ml CHX and prepared as described above for the runoff experiment. Preparation of polysomes from the wild-type and $uL10_{\Delta h1h2}$ mutant yeast cells in the presence of Sor was performed under standard conditions, except that CHX was replaced with Sor (40 μg/ml). To analyze the effect of the sublethal dose of CHX, the cells were grown in YPD medium overnight and diluted to an OD_{600} of 0.1, 50 ng/ml of CHX was added, and the cells were grown to an OD_{600} of 0.4 to 0.6 at 30°C. Polysome and runoff analyses were performed as described above, except in the runoff experiments, in which 50 ng/ml of CHX was present in all buffers. Mathematical analyses of polysome profiles were conducted using MicrocalOrigin 6.0 software. The area of polysome fractions was calculated by the integration method to assess the total surface area and to determine the polysome-to-monosome (P/M) and 40S/60S ratios. For immune detection, the cells were disrupted with glass beads at 4°C in 10 mM Tris-HCl (pH 7.5)–100 mM NaCl–30 mM $MgCl_2$ buffer and cleared by centrifugation at 12,000 rpm, and, where desired, the proteins from specific fractions were precipitated with 10% trichloroacetic acid (TCA) and analyzed by SDS-PAGE, followed by electrotransfer onto an immobilization membrane. Specific antibodies directed against uL10 were used as described previously (25); antibodies against uL23 were kindly provided by Ed Hurt.

Determination of translational fitness by incorporation of ^{35}S-radiolabeled methionine. The cells were grown to an OD_{600} of 0.4 to 0.6, washed with deionized water, and resuspended with methionine-depleted SD minimal medium. The cells were cultivated at 30°C for 15 min, unlabeled methionine was added to a final concentration of 50 μM, and 37 kBq of [^{35}S]methionine (37 TBq/mmol; Hartmann Analytics) was added at time zero (T_0). The OD_{600} of the cultures was measured at 10-min intervals, and 1-ml aliquots of the cultures were collected. Total proteins were precipitated with ice-cold 10% TCA (final concentration), collected on Whatman GF/C filters, and counted in a scintillation counter (Beckman LS6000SE). The translation impairment was determined by comparison of the incorporation rates (cpm/OD_{600}/min) of mutant and wild-type cells. For the measurement of the effect of inhibitors on translation efficiency, the overnight cultures were diluted to an OD_{600} of 0.1 on SD minimal medium, grown for 1 h, and subsequently treated with indicated antibiotics; the cells were grown to an OD_{600} of 0.4 to 0.6 at 30°C before the pulse-chase procedure.

The determination of the ribosome half-transit time was based on a comparison of the rates of [^{35}S]methionine incorporation into total (nascent and completed) and completed proteins. Briefly, 10 ml of yeast culture (grown under conditions as described above for the pulse-chase procedure) was harvested at each time point (0, 2, 4, 6, 8, 10, 12, and 14 min) and resuspended in 500 μl of lysis buffer (10 mM Tris-HCl [pH 7.4], 100 mM NaCl, 30 mM $MgCl_2$, 200 μg/ml heparin, 100 μg/ml CHX, 1 mM PMSF, 6 mM β-mercaptoethanol). The cells were then disrupted by vigorous shaking with an equal volume of glass beads. Cell debris was removed by centrifugation (12,000 rpm, 4°C, 20 min). The supernatant was divided into two equal parts. The first part, i.e., the total protein fraction, was precipitated with ice-cold 10% TCA, collected on Whatman GF/C filters, and counted in a scintillation counter. The second part was ultracentrifuged at 105,000 $\times$ g for 45 min to obtain a postribosomal fraction and analyzed in the same way. The radioactivities (expressed in counts/minute) of the total protein fraction and the postribosomal fraction were plotted as a function of time. Ribosome half-transit time ($t_{1/2}$) was determined from the displacement in time between two trend lines delineated for each data series and obtained by linear regression analysis as described previously (70).

Quantification of frameshifting and missense and nonsense errors using the dual-luciferase assay. The efficiency of programmed ribosome frameshifting (PRF) was determined using the dual-luciferase assay according to an established procedure (50). Briefly, each yeast strain was transformed with control plasmid pYDL and with appropriate vectors to measure -1 PRF (pYDL-LA) and $+1$ PRF (pYDL-Ty*1*), respectively (kindly provided by Jonathan Dinman). Initially, the selected transformants were grown on liquid SD minimal medium without uracil overnight at 30°C, diluted with fresh prewarmed medium to an OD_{600} of 0.2, and further cultivated until the OD_{600} reached 0.5. The cells were then collected by centrifugation, washed with ice-cold PBS, and disrupted by vortexing with glass beads in ice-cold PBS buffer supplemented with 1 mM PMSF, 5 mM dithiothreitol (DTT), and 1 mg/ml porcine

gelatin (Sigma-Aldrich). The cell extracts were precleared by centrifugation at 10,000 × *g* for 10 min. To analyze the effect of translational inhibitors, logarithmically growing cells were treated with the antibiotic G418 (100 or 200 μg/ml) for 5 h before extract preparation. Luciferase activity was quantified using the Dual-Luciferase reporter assay system (Promega) according to the manufacturer's instructions, except that 2 μl of the cell extract was added to 20 μl of LAR II reagent and 20 μl of Stop&Glow reagent was subsequently added to the mixture. The level of respective decoding impairment was expressed as the firefly/*Renilla* luciferase activity ratio obtained for the test vector divided by the firefly/*Renilla* luciferase activity ratio obtained for the control vector, multiplied by 100%. The results are an average result for three independent biological experiments. The following genetic constructs were used: for misincorporation, pDB688, a control plasmid with a cognate CAC codon encoding His amino acid at position 245 of firefly luciferase; pDB866, with near-cognate CAG (245 Gln); pDB868, with near-cognate CGC (245 Arg); and pDB866-MT (modified in our laboratory), having CGA (245 Arg), which can be regarded as a noncognate codon (underlined nucleotides indicate mutations within the CAC codon); for readthrough, pDB688, a control plasmid with sequence CAAA and pDB691 with stop signal UGAC. All plasmids were kindly provided by David Bedwell (52). The following constructs were also used: for misincorporation, pJD375, a control plasmid with cognate AGA (218 Arg) at position 218 of firefly luciferase, and pJD643, with near-cognate AGC (218 Ser) and pJD642 with noncognate TCT (218 Ser); for frameshifting, pJD375, a control plasmid; pJD376, −1 PRF (L-A); and pJD377, +1 PRF (Ty*1*). All vectors were kindly provided by Jonathan Dinman (53).

Cell cycle analysis using flow cytometry. A total of 4 × 10^6 cells were harvested by centrifugation and resuspended in 1 ml of 70% ethanol upon slow mixing. After 1 h of ethanol fixation at room temperature, 0.3 ml of the cell suspension was washed with 50 mM sodium citrate, pH 7.5, centrifuged, and then resuspended in 1 ml of RNase solution (0.25 mg/ml RNase in 50 mM sodium citrate, pH 7.5) (Sigma-Aldrich). After overnight incubation at 37°C, proteinase K (A&A Biotechnology) was added to a final concentration of 200 μg/ml and the samples were incubated for 1.5 h at 50°C. After the addition of propidium iodide (PI; 8 μg/ml) (Sigma-Aldrich), the samples were kept in the dark for 30 min at room temperature. Cell cycle analysis was performed on a BD FACSVerse system (BD Biosciences), and data were analyzed using BD FACSuite software (BD Biosciences). Ten thousand cells were analyzed per strain in triplicate, and three independent biological experiments were performed.

Miscellaneous. Isoelectrofocusing electrophoresis (IEF) of ribosomal proteins was carried out on slab gel analysis in a 2.5 to 5.0 pH range and with silver staining (28). The ribosome concentration was established according to reference 71. The protein concentration was measured according to Bradford using a Bio-Rad protein assay kit.

SUPPLEMENTAL MATERIAL

Supplemental material for this article may be found at https://doi.org/10.1128/MCB.00060-17.

SUPPLEMENTAL FILE 1, PDF file, 0.3 MB.

ACKNOWLEDGMENTS

We gratefully acknowledge the use of the facilities of the Ecotech-Complex in Lublin, under project number UDA-POIG.02.01.00-06-212/09-03. We are indebted to Marina Rodnina for critical reading of the manuscript.

This work was supported by a grant from the National Science Center in Poland (UMO-2014/13/B/NZ1/00953) to M.T.

We declare that they we have no conflicts of interest with the contents of this article.

L.W. designed, analyzed, and interpreted the data and wrote the manuscript, E.M. contributed to Fig. 1B, 2 through 7, and 9, M.S. contributed to Fig. 7 and 8, B.M.-W. contributed to Fig. 1D, M.M. contributed to Fig. 1C, P.G. contributed to Fig. 1A and 9A, A.B. contributed to Fig. 2, L.B. contributed to Fig. 7, and M.T. conceived the study, analyzed and interpreted the data, and wrote the manuscript.

REFERENCES

1. Maracci C, Rodnina MV. 2016. Review: translational GTPases. Biopolymers 105:463–475. https://doi.org/10.1002/bip.22832.
2. Liljas A, Ehrenberg M. 2013. Structural aspects of protein synthesis, 2nd ed. World Scientific, Singapore.
3. Diaconu M, Kothe U, Schlunzen F, Fischer N, Harms JM, Tonevitsky AG, Stark H, Rodnina MV, Wahl MC. 2005. Structural basis for the function of the ribosomal L7/12 stalk in factor binding and GTPase activation. Cell 121:991–1004. https://doi.org/10.1016/j.cell.2005.04.015.
4. Wahl MC, Moller W. 2002. Structure and function of the acidic ribosomal stalk proteins. Curr Protein Pept Sci 3:93–106. https://doi.org/10.2174/1389203023380756.
5. Gonzalo P, Reboud JP. 2003. The puzzling lateral flexible stalk of the ribosome. Biol Cell 95:179–193. https://doi.org/10.1016/S0248-4900(03)00034-0.
6. Ballesta JP, Remacha M. 1996. The large ribosomal subunit stalk as a regulatory element of the eukaryotic translational machinery. Prog Nucleic Acid Res Mol Biol 55:157–193. https://doi.org/10.1016/S0079-6603(08)60193-2.
7. Tchorzewski M. 2002. The acidic ribosomal P proteins. Int J Biochem Cell Biol 34:911–915. https://doi.org/10.1016/S1357-2725(02)00012-2.
8. Grela P, Bernado P, Svergun D, Kwiatowski J, Abramczyk D, Grankowski N, Tchorzewski M. 2008. Structural relationships among the ribosomal

stalk proteins from the three domains of life. J Mol Evol 67:154–167. https://doi.org/10.1007/s00239-008-9132-2.
9. Helgstrand M, Mandava CS, Mulder FA, Liljas A, Sanyal S, Akke M. 2007. The ribosomal stalk binds to translation factors IF2, EF-Tu, EF-G and RF3 via a conserved region of the L12 C-terminal domain. J Mol Biol 365:468–479. https://doi.org/10.1016/j.jmb.2006.10.025.
10. Nomura N, Honda T, Baba K, Naganuma T, Tanzawa T, Arisaka F, Noda M, Uchiyama S, Tanaka I, Yao M, Uchiumi T. 2012. Archaeal ribosomal stalk protein interacts with translation factors in a nucleotide-independent manner via its conserved C terminus. Proc Natl Acad Sci U S A 109:3748–3753. https://doi.org/10.1073/pnas.1112934109.
11. Leijonmarck M, Liljas A. 1987. Structure of the C-terminal domain of the ribosomal protein L7/L12 from Escherichia coli at 1.7 A. J Mol Biol 195:555–579. https://doi.org/10.1016/0022-2836(87)90183-5.
12. Bocharov EV, Sobol AG, Pavlov KV, Korzhnev DM, Jaravine VA, Gudkov AT, Arseniev AS. 2004. From structure and dynamics of protein L7/L12 to molecular switching in ribosome. J Biol Chem 279:17697–17706. https://doi.org/10.1074/jbc.M313384200.
13. Grela P, Helgstrand M, Krokowski D, Boguszewska A, Svergun D, Liljas A, Bernado P, Grankowski N, Akke M, Tchorzewski M. 2007. Structural characterization of the ribosomal P1A-P2B protein dimer by small-angle X-ray scattering and NMR spectroscopy. Biochemistry 46:1988–1998. https://doi.org/10.1021/bi0616450.
14. Lee KM, Yu CW, Chiu TY, Sze KH, Shaw PC, Wong KB. 2012. Solution structure of the dimerization domain of the eukaryotic stalk P1/P2 complex reveals the structural organization of eukaryotic stalk complex. Nucleic Acids Res 40:3172–3182. https://doi.org/10.1093/nar/gkr1143.
15. Naganuma T, Nomura N, Yao M, Mochizuki M, Uchiumi T, Tanaka I. 2010. Structural basis for translation factor recruitment to the eukaryotic/archaeal ribosomes. J Biol Chem 285:4747–4756. https://doi.org/10.1074/jbc.M109.068098.
16. Mulder FA, Bouakaz L, Lundell A, Venkataramana M, Liljas A, Akke M, Sanyal S. 2004. Conformation and dynamics of ribosomal stalk protein L12 in solution and on the ribosome. Biochemistry 43:5930–5936. https://doi.org/10.1021/bi0495331.
17. Bernado P, Modig K, Grela P, Svergun DI, Tchorzewski M, Pons M, Akke M. 2010. Structure and dynamics of ribosomal protein L12: an ensemble model based on SAXS and NMR relaxation. Biophys J 98:2374–2382. https://doi.org/10.1016/j.bpj.2010.02.012.
18. Oleinikov AV, Jokhadze GG, Traut RR. 1998. A single-headed dimer of Escherichia coli ribosomal protein L7/L12 supports protein synthesis. Proc Natl Acad Sci U S A 95:4215–4218. https://doi.org/10.1073/pnas.95.8.4215.
19. Santos C, Ballesta JP. 1995. The highly conserved protein P0 carboxyl end is essential for ribosome activity only in the absence of proteins P1 and P2. J Biol Chem 270:20608–20614. https://doi.org/10.1074/jbc.270.35.20608.
20. Davydov II, Wohlgemuth I, Artamonova II, Urlaub H, Tonevitsky AG, Rodnina MV. 2013. Evolution of the protein stoichiometry in the L12 stalk of bacterial and organellar ribosomes. Nat Commun 4:1387. https://doi.org/10.1038/ncomms2373.
21. Gordiyenko Y, Videler H, Zhou M, McKay AR, Fucini P, Biegel E, Muller V, Robinson CV. 2010. Mass spectrometry defines the stoichiometry of ribosomal stalk complexes across the phylogenetic tree. Mol Cell Proteomics 9:1774–1783. https://doi.org/10.1074/mcp.M000072-MCP201.
22. Maki Y, Hashimoto T, Zhou M, Naganuma T, Ohta J, Nomura T, Robinson CV, Uchiumi T. 2007. Three binding sites for stalk protein dimers are generally present in ribosomes from archaeal organism. J Biol Chem 282:32827–32833. https://doi.org/10.1074/jbc.M705412200.
23. Tchorzewski M, Boldyreff B, Issinger O, Grankowski N. 2000. Analysis of the protein-protein interactions between the human acidic ribosomal P-proteins: evaluation by the two hybrid system. Int J Biochem Cell Biol 32:737–746. https://doi.org/10.1016/S1357-2725(00)00017-0.
24. Tchorzewski M, Boguszewska A, Dukowski P, Grankowski N. 2000. Oligomerization properties of the acidic ribosomal P-proteins from Saccharomyces cerevisiae: effect of P1A protein phosphorylation on the formation of the P1A-P2B hetero-complex. Biochim Biophys Acta 1499:63–73. https://doi.org/10.1016/S0167-4889(00)00108-7.
25. Krokowski D, Boguszewska A, Abramczyk D, Liljas A, Tchorzewski M, Grankowski N. 2006. Yeast ribosomal P0 protein has two separate binding sites for P1/P2 proteins. Mol Microbiol 60:386–400. https://doi.org/10.1111/j.1365-2958.2006.05117.x.
26. Hagiya A, Naganuma T, Maki Y, Ohta J, Tohkairin Y, Shimizu T, Nomura T, Hachimori A, Uchiumi T. 2005. A mode of assembly of P0, P1, and P2 proteins at the GTPase-associated center in animal ribosome: in vitro analyses with P0 truncation mutants. J Biol Chem 280:39193–39199. https://doi.org/10.1074/jbc.M506050200.
27. Perez-Fernandez J, Remacha M, Ballesta JP. 2005. The acidic protein binding site is partially hidden in the free Saccharomyces cerevisiae ribosomal stalk protein P0. Biochemistry 44:5532–5540. https://doi.org/10.1021/bi047332r.
28. Grela P, Krokowski D, Gordiyenko Y, Krowarsch D, Robinson CV, Otlewski J, Grankowski N, Tchorzewski M. 2010. Biophysical properties of the eukaryotic ribosomal stalk. Biochemistry 49:924–933. https://doi.org/10.1021/bi901811s.
29. Tchorzewski M, Krokowski D, Boguszewska A, Liljas A, Grankowski N. 2003. Structural characterization of yeast acidic ribosomal P proteins forming the P1A-P2B heterocomplex. Biochemistry 42:3399–3408. https://doi.org/10.1021/bi0206006.
30. Remacha M, Jimenez-Diaz A, Bermejo B, Rodriguez-Gabriel MA, Guarinos E, Ballesta JP. 1995. Ribosomal acidic phosphoproteins P1 and P2 are not required for cell viability but regulate the pattern of protein expression in Saccharomyces cerevisiae. Mol Cell Biol 15:4754–4762. https://doi.org/10.1128/MCB.15.9.4754.
31. Martinez-Azorin F, Remacha M, Ballesta JP. 2008. Functional characterization of ribosomal P1/P2 proteins in human cells. Biochem J 413:527–534. https://doi.org/10.1042/BJ20080049.
32. Harms JM, Wilson DN, Schluenzen F, Connell SR, Stachelhaus T, Zaborowska Z, Spahn CM, Fucini P. 2008. Translational regulation via L11: molecular switches on the ribosome turned on and off by thiostrepton and micrococcin. Mol Cell 30:26–38. https://doi.org/10.1016/j.molcel.2008.01.009.
33. Gao YG, Selmer M, Dunham CM, Weixlbaumer A, Kelley AC, Ramakrishnan V. 2009. The structure of the ribosome with elongation factor G trapped in the posttranslocational state. Science 326:694–699. https://doi.org/10.1126/science.1179709.
34. Datta PP, Sharma MR, Qi L, Frank J, Agrawal RK. 2005. Interaction of the G′ domain of elongation factor G and the C-terminal domain of ribosomal protein L7/L12 during translocation as revealed by cryo-EM. Mol Cell 20:723–731. https://doi.org/10.1016/j.molcel.2005.10.028.
35. Schmeing TM, Ramakrishnan V. 2009. What recent ribosome structures have revealed about the mechanism of translation. Nature 461:1234–1242. https://doi.org/10.1038/nature08403.
36. Murray J, Savva CG, Shin BS, Dever TE, Ramakrishnan V, Fernandez IS. 2016. Structural characterization of ribosome recruitment and translocation by type IV IRES. eLife 5:e13567.
37. Voorhees RM, Schmeing TM, Kelley AC, Ramakrishnan V. 2010. The mechanism for activation of GTP hydrolysis on the ribosome. Science 330:835–838. https://doi.org/10.1126/science.1194460.
38. Fischer N, Neumann P, Bock LV, Maracci C, Wang Z, Paleskava A, Konevega AL, Schroder GF, Grubmuller H, Ficner R, Rodnina MV, Stark H. 2016. The pathway to GTPase activation of elongation factor SelB on the ribosome. Nature 540:80–85. https://doi.org/10.1038/nature20560.
39. Pallesen J, Hashem Y, Korkmaz G, Koripella RK, Huang C, Ehrenberg M, Sanyal S, Frank J. 2013. Cryo-EM visualization of the ribosome in termination complex with apo-RF3 and RF1. eLife 2:e00411. https://doi.org/10.7554/eLife.00411.
40. Chen Y, Feng S, Kumar V, Ero R, Gao YG. 2013. Structure of EF-G-ribosome complex in a pretranslocation state. Nat Struct Mol Biol 20:1077–1084. https://doi.org/10.1038/nsmb.2645.
41. Mohr D, Wintermeyer W, Rodnina MV. 2002. GTPase activation of elongation factors Tu and G on the ribosome. Biochemistry 41:12520–12528. https://doi.org/10.1021/bi026301y.
42. Pape T, Wintermeyer W, Rodnina MV. 1998. Complete kinetic mechanism of elongation factor Tu-dependent binding of aminoacyl-tRNA to the A site of the E. coli ribosome. EMBO J 17:7490–7497. https://doi.org/10.1093/emboj/17.24.7490.
43. Johansson M, Bouakaz E, Lovmar M, Ehrenberg M. 2008. The kinetics of ribosomal peptidyl transfer revisited. Mol Cell 30:589–598. https://doi.org/10.1016/j.molcel.2008.04.010.
44. Kothe U, Wieden HJ, Mohr D, Rodnina MV. 2004. Interaction of helix D of elongation factor Tu with helices 4 and 5 of protein L7/12 on the ribosome. J Mol Biol 336:1011–1021. https://doi.org/10.1016/j.jmb.2003.12.080.
45. Savelsbergh A, Mohr D, Kothe U, Wintermeyer W, Rodnina MV. 2005. Control of phosphate release from elongation factor G by ribosomal protein L7/12. EMBO J 24:4316–4323. https://doi.org/10.1038/sj.emboj.7600884.

46. Baba K, Tumuraya K, Tanaka I, Yao M, Uchiumi T. 2013. Molecular dissection of the silkworm ribosomal stalk complex: the role of multiple copies of the stalk proteins. Nucleic Acids Res 41:3635–3643. https://doi.org/10.1093/nar/gkt044.
47. Shimizu T, Nakagaki M, Nishi Y, Kobayashi Y, Hachimori A, Uchiumi T. 2002. Interaction among silkworm ribosomal proteins P1, P2 and P0 required for functional protein binding to the GTPase-associated domain of 28S rRNA. Nucleic Acids Res 30:2620–2627. https://doi.org/10.1093/nar/gkf379.
48. Uchiumi T, Honma S, Nomura T, Dabbs ER, Hachimori A. 2002. Translation elongation by a hybrid ribosome in which proteins at the GTPase center of the Escherichia coli ribosome are replaced with rat counterparts. J Biol Chem 277:3857–3862. https://doi.org/10.1074/jbc.M107730200.
49. Kryndushkin DS, Smirnov VN, Ter-Avanesyan MD, Kushnirov VV. 2002. Increased expression of Hsp40 chaperones, transcriptional factors, and ribosomal protein Rpp0 can cure yeast prions. J Biol Chem 277:23702–23708. https://doi.org/10.1074/jbc.M111547200.
50. Harger JW, Dinman JD. 2003. An in vivo dual-luciferase assay system for studying translational recoding in the yeast Saccharomyces cerevisiae. RNA 9:1019–1024. https://doi.org/10.1261/rna.5930803.
51. Kramer EB, Farabaugh PJ. 2007. The frequency of translational misreading errors in E. coli is largely determined by tRNA competition. RNA 13:87–96. https://doi.org/10.1261/rna.294907.
52. Salas-Marco J, Bedwell DM. 2005. Discrimination between defects in elongation fidelity and termination efficiency provides mechanistic insights into translational readthrough. J Mol Biol 348:801–815. https://doi.org/10.1016/j.jmb.2005.03.025.
53. Plant EP, Nguyen P, Russ JR, Pittman YR, Nguyen T, Quesinberry JT, Kinzy TG, Dinman JD. 2007. Differentiating between near- and non-cognate codons in Saccharomyces cerevisiae. PLoS One 2:e517. https://doi.org/10.1371/journal.pone.0000517.
54. Wilson DN. 2009. The A-Z of bacterial translation inhibitors. Crit Rev Biochem Mol Biol 44:393–433. https://doi.org/10.3109/10409230903307311.
55. Ito K, Honda T, Suzuki T, Miyoshi T, Murakami R, Yao M, Uchiumi T. 2014. Molecular insights into the interaction of the ribosomal stalk protein with elongation factor 1alpha. Nucleic Acids Res 42:14042–14052. https://doi.org/10.1093/nar/gku1248.
56. Savelsbergh A, Mohr D, Wilden B, Wintermeyer W, Rodnina MV. 2000. Stimulation of the GTPase activity of translation elongation factor G by ribosomal protein L7/12. J Biol Chem 275:890–894. https://doi.org/10.1074/jbc.275.2.890.
57. Connell SR, Takemoto C, Wilson DN, Wang H, Murayama K, Terada T, Shirouzu M, Rost M, Schuler M, Giesebrecht J, Dabrowski M, Mielke T, Fucini P, Yokoyama S, Spahn CM. 2007. Structural basis for interaction of the ribosome with the switch regions of GTP-bound elongation factors. Mol Cell 25:751–764. https://doi.org/10.1016/j.molcel.2007.01.027.
58. Stark H, Rodnina MV, Rinke-Appel J, Brimacombe R, Wintermeyer W, van Heel M. 1997. Visualization of elongation factor Tu on the Escherichia coli ribosome. Nature 389:403–406. https://doi.org/10.1038/38770.
59. Tourigny DS, Fernandez IS, Kelley AC, Ramakrishnan V. 2013. Elongation factor G bound to the ribosome in an intermediate state of translocation. Science 340:1235490. https://doi.org/10.1126/science.1235490.
60. Rodnina MV, Wintermeyer W. 2016. Protein elongation, co-translational folding and targeting. J Mol Biol 428:2165–2185. https://doi.org/10.1016/j.jmb.2016.03.022.
61. Zinker S, Warner JR. 1976. The ribosomal proteins of Saccharomyces cerevisiae. Phosphorylated and exchangeable proteins. J Biol Chem 251:1799–1807.
62. Rodnina MV, Pape T, Fricke R, Kuhn L, Wintermeyer W. 1996. Initial binding of the elongation factor Tu.GTP.aminoacyl-tRNA complex preceding codon recognition on the ribosome. J Biol Chem 271:646–652. https://doi.org/10.1074/jbc.271.2.646.
63. Blanchard SC, Gonzalez RL, Kim HD, Chu S, Puglisi JD. 2004. tRNA selection and kinetic proofreading in translation. Nat Struct Mol Biol 11:1008–1014. https://doi.org/10.1038/nsmb831.
64. Wawiorka L, Molestak E, Szajwaj M, Michalec-Wawiorka B, Boguszewska A, Borkiewicz L, Liudkovska V, Kufel J, Tchorzewski M. 2016. Functional analysis of the uL11 protein impact on translational machinery. Cell Cycle 15:1060–1072. https://doi.org/10.1080/15384101.2016.1154245.
65. Peske F, Kuhlenkoetter S, Rodnina MV, Wintermeyer W. 2014. Timing of GTP binding and hydrolysis by translation termination factor RF3. Nucleic Acids Res 42:1812–1820. https://doi.org/10.1093/nar/gkt1095.
66. Goyal A, Belardinelli R, Maracci C, Milon P, Rodnina MV. 2015. Directional transition from initiation to elongation in bacterial translation. Nucleic Acids Res 43:10700–10712. https://doi.org/10.1093/nar/gkv869.
67. Savelsbergh A, Katunin VI, Mohr D, Peske F, Rodnina MV, Wintermeyer W. 2003. An elongation factor G-induced ribosome rearrangement precedes tRNA-mRNA translocation. Mol Cell 11:1517–1523. https://doi.org/10.1016/S1097-2765(03)00230-2.
68. Harger JW, Meskauskas A, Dinman JD. 2002. An "integrated model" of programmed ribosomal frameshifting. Trends Biochem Sci 27:448–454. https://doi.org/10.1016/S0968-0004(02)02149-7.
69. Molon M, Szajwaj M, Tchorzewski M, Skoczowski A, Niewiadomska E, Zadrag-Tecza R. 2016. The rate of metabolism as a factor determining longevity of the Saccharomyces cerevisiae yeast. Age (Dordr) 38:11. https://doi.org/10.1007/s11357-015-9868-8.
70. Ruvinsky I, Sharon N, Lerer T, Cohen H, Stolovich-Rain M, Nir T, Dor Y, Zisman P, Meyuhas O. 2005. Ribosomal protein S6 phosphorylation is a determinant of cell size and glucose homeostasis. Genes Dev 19:2199–2211. https://doi.org/10.1101/gad.351605.
71. van der Zeijst BA, Kool AJ, Bloemers HP. 1972. Isolation of active ribosomal subunits from yeast. Eur J Biochem 30:15–25. https://doi.org/10.1111/j.1432-1033.1972.tb02066.x.